THE JOURNAL OF BIOLOGICAL CHEMISTRY VOL. 292, NO. 9, pp. 3568–3580, March 3, 2017

Dual Functional Roles of Molecular Beacon as a MicroRNA Detector and Inhibitor*[S]

Received for publication, November 2, 2016, and in revised form, January 4, 2017 Published, JBC Papers in Press, January 18, 2017, DOI 10.1074/jbc.M116.765776

Wai Ming Li[‡], Ching-Man Chan[§], Andrew L. Miller[§], and Chow H. Lee[‡1]

From the [‡]Chemistry Program, University of Northern British Columbia, Prince George, British Columbia V2N 4Z9, Canada and the [§]Division of Life Science and Key State Laboratory for Molecular Neuroscience, Hong Kong University of Science and Technology, Clear Water Bay, Kowloon, Hong Kong

Edited by Xiao-Fan Wang

MicroRNAs are essential in many cellular processes. The ability to detect microRNAs is important for understanding its function and biogenesis. This study is aimed at using a molecular beacon to detect miR-430 in developing zebrafish embryos as a proof of principle. miR-430 is crucial for the clearance of maternal mRNA during maternal zygotic transition in embryonic development. Despite its known function, the temporal and spatial expression of miR-430 remains unclear. We used various imaging techniques, including laser scanning confocal microscopy, spinning disk, and lightsheet microscopy, to study the localization of miR-430 and any developmental defects possibly caused by the molecular beacon. Our results show that miR-430 is expressed early in development and is localized in distinct cytoplasmic granules where its target mRNA can be detected. We also show that the designed molecular beacon can inhibit the function of miR-430 and cause developmental defect in the brain, notochord, heart, and kidney, depending on the delivery site within the embryo, suggesting that miR-430 plays a diverse role in embryonic morphogenesis. When compared with morpholino, molecular beacon is 2 orders of magnitude more potent in inhibiting miR-430. Thus, our results reveal that in addition to being used as a valuable tool for the detection of microRNAs *in vivo*, molecular beacons can also be employed to inhibit microRNAs in a specific manner.

MicroRNAs (miRNAs)[2] are a class of short, non-coding RNAs involved in the regulation of gene expression at the post-transcriptional level. MiRNAs are implicated in many diseases and are essential in many cellular processes including development (1). Understanding the spatial expression of these small RNAs inside the cell can provide important information about their molecular function. The use of *in situ* hybridization to study intracellular localization of miRNAs in fixed cells has technical limitations because of the small size and low quantities of the RNA (2). In addition, an unusual high background, possibly contributed by nonspecific binding to DNA, can make interpretation of results difficult (3). Live imaging of miRNAs has been attempted in many studies, but success remains questionable, mainly because of challenges in the delivery of miRNA sensors to the appropriate compartment inside the cell. Most sensors were introduced into cells using a lipid-based delivery system, which may bias the delivery of the sensors to the endocytic pathway of the cell destined for degradation. In fact, the pattern of miRNA expression in punctate structures shown by these studies differs substantially from *in situ* hybridization experiments (3–10). Among the many types of sensors used in tracking miRNAs, molecular beacons hold the greatest promise because of their high specificity toward small sequences of RNA and low signal to noise ratio (11, 12). Furthermore, molecular beacons are able to provide real time signals without relying on other indirect and complicated detection systems such as fluorescent or bioluminescent protein-based systems (6–7, 13–15). Because of the aforementioned obstacles, the usefulness of molecular beacons for the real time imaging of miRNA in live cells remains uncertain. This study was aimed at using a molecular beacon and the developing zebrafish embryo to track the expression of miR-430 as a proof of principle. To avoid bias in the results caused by delivery, the molecular beacon was introduced into the large cells of the zebrafish embryo by microinjection.

Molecular beacons are short oligonucleotide sequences with a stem-loop structure (see Fig. 1*A*) containing a single-stranded loop region that is antisense to the target sequence to be detected (11). The loop region is flanked by two short sequences, usually four to seven nucleotides, which are self-complementary and form the double-stranded stem region of the beacon. Attached to the 5′ and 3′ ends of a molecular beacon are a fluorophore and a quencher. In the absence of the target sequence, the molecular beacon is in its closed conformation with the quencher in close proximity to the fluorophore thus emitting low fluorescence signal. Upon hybridization to a specific target sequence, the molecular beacon is in its open conformation, and the fluorophore is no longer quenched thus emitting a strong signal. Disruption of the secondary structure of the molecular beacon forms the basis for its ability to detect oligonucleotides with a low signal to background ratio. The

* This work was supported by Natural Sciences & Engineering Research Council Discovery Grant 227158 (to C. H. L.), Hong Kong Research Grant Council (RGC) General Research Fund Awards 662113, 16101714, and 16100115, and Hong Kong Innovation and Technology Commission Grant ITCPD/17-9 (to A. L. M.). The authors declare that they have no conflicts of interest with the contents of this article.

[S] This article contains supplemental Fig. S1 and Movies S1 and S2.

[1] To whom correspondence should be addressed: Chemistry Program, University of Northern British Columbia, 3333 University Way, Prince George, BC V2N 4Z9, Canada. Tel.: 250-960-5413; Fax: 250-960-5845; E-mail: chow.lee@unbc.ca.

[2] The abbreviations used are: miRNA, microRNA; hpf, h postfertilization; dpf, days postfertilization; qPCR, quantitative PCR; MZT, maternal zygotic transition; SSC, saline-sodium citrate; 6-FAM, 6-fluorescein amidite; MO, morpholino.

ability of molecular beacons to quantify miRNAs in a highly sensitive and sequence-specific manner has been previously demonstrated *in vitro* (16).

In the zebrafish (*Danio rerio*), only a few miRNAs are expressed during early development, and some of them are essential (17). Among them, miR-430 has been shown to be highly expressed as early as 2.5 h postfertilization (hpf) (17) and is required for the degradation of maternal mRNA during maternal zygotic transition (MZT) (18). Such function of miR-430 was also demonstrated by its ortholog (miR-427) in *Xenopus* (19). MiR-430 is also involved in germ layer specification through its role in regulating nodal signaling (20, 21). Although the mechanism of how miR-430 functions to control the cascade of events leading to the massive turnover of maternal mRNA remains largely unclear, the lack of this miRNA eventually causes defects in brain development (22). In the zebrafish, the miR-430 family has several members including miR-430a, miR-430b, miR-430c, and miR-430i with multiple genes encoding each of the miR-430 members (22–24). Because miR-430 plays such an important role in development, it would be of interest to study the spatial and temporal expression of this miRNA in more detail. Using the zebrafish embryo as a model system, we are able to demonstrate the usefulness of a molecular beacon to track a specific miRNA *in vivo* as a proof of principle. Our results also unexpectedly show that molecular beacon can be used as a strong miRNA inhibitor for studying development.

Results

Specificity of MB-miR430b—A molecular beacon with a fluorophore and a quencher was designed to detect miR-430b in the zebrafish embryo (Fig. 1*A*). For simplicity, MB-miR430b is named as MB for the rest of this paper. As shown in Fig. 1 (*B–E*), an increase in fluorescence signal caused by dequenching occurs in the presence of RNA or DNA oligonucleotides having bases complementary to the loop region of MB. Binding of MB to its target molecule is dependent on time as well as the concentration of the target molecule (Fig. 1, *B* and *C*). The binding of MB to its target was shown to occur faster if the target molecule is made with DNA rather than RNA (Fig. 1*E*, *blue versus red*). To determine the sequence specificity of MB, target molecules belonging to the miR-430 family, but with mismatches (Fig. 1*A*), were also tested. Mismatches in the target molecules with DNA backbone were shown to completely abolish the binding of MB, whereas mismatches in RNA target appears to have a less impact on binding (Fig. 1, *D* and *E*). For instance, miR-430c-RNA was still able to bind to MB but as compared with miR-430b-RNA, the rate of binding was substantially lower (Fig. 1*E*). To determine the stability of the various hybrids formed upon binding of the MB to different target molecules, melting curves of the hybrids were generated (Fig. 1*F*). As shown, the melting temperature (T_M) of MB in buffer (79 °C) did not change when miR-430a-DNA, miR-430c-DNA and miR-430i-DNA were present, confirming that these molecules do not bind to MB. When miR-430b-DNA was present, the T_M was reduced to 53 °C, which is considerably lower than the T_M of the hybrid with miR-430b-RNA of 74 °C, confirming that a change in the backbone of the target molecule from RNA to DNA does lower the affinity of binding. Also, a lower T_M obtained with miR-430c-RNA (51 °C) also confirms that mismatches in the RNA sequence does contribute to lower stability of the duplex.

MB Localization in Early Development—Previous studies have shown that miR-430 is expressed as early as 2.5 hpf in zebrafish embryos as detected by microarray analysis (17). We are interested to see whether miR-430 can be detected at a much earlier time using a molecular beacon. When MB was injected at the 1-cell stage in zebrafish embryos, a nuclear signal, as well as diffuse cytoplasmic signal, was observed at the 16-cell stage (1.5 hpf) (Fig. 2*A*), suggesting that MB was localized predominantly in the nucleus. At 4 hpf, MB is localized in the nucleus, as well as in granular structures in the cytoplasm (Fig. 2*B*). As a control, we injected another molecular beacon with the loop region complementary to a piRNA (piR-dre-210905), which is expressed as early as the 256-cell stage (17). We found that the piRNA is localized in the nucleus but not in granular structures within the cytoplasm (Fig. 2, *C* and *D*). The cellular distribution of MB was followed in a time series experiment after 4 hpf when the cytoplasmic granules are visible (Fig. 2, *E–H*). During parts of the cell cycle, MB localization in the nucleus disappeared and reappeared as the nuclei were disassembled (*white*, *red*, and *pink arrows*) and reassembled (*white*, *red*, and *pink arrowheads*). As the nuclear signal disappeared in each cell cycle, there was an increase in the overall signal throughout the cell, suggesting the target-bound MB is no longer confined to the nucleus (Fig. 2, *F* and *G*). In contrast, MB localization in cytoplasmic granules did not appear to be affected by the cell cycle and remained visible when the nucleus was disassembled. To determine whether nuclear localization of MB is due to nonspecific binding of MB to chromatin, another molecular beacon that targets to a human c-Myc sequence was included as a control (supplemental Fig. S1). Nuclear localization of this control beacon was found to be minimal, suggesting that nuclear localization of MB is specific. Next we tested whether the nuclear localization of MB is due to binding to miR-430 gene or miR-430 precursors by performing transcriptional inhibition experiments using actinomycin D. Because MB can bind to complementary sequence with DNA backbone (Fig. 1), it may be possible that MB is binding to miR-430 precursors, as well as DNA sequences in the genome encoding the microRNA. Actinomycin D was microinjected at the 1-cell stage, and cell division was not affected within the period for imaging MB (Fig. 2*I*). As shown by the complete abolishment of the nuclear signal in the absence of transcription (Fig. 2, compare *B* with *I*), our results suggest that nuclear localization of MB is due to MB binding to miR-430 or its precursors but not the miRNA genes. Cytoplasmic granules were also abolished as miRNA biogenesis was stopped because of transcriptional inhibition (Fig. 2, compare *B* with *I*). To determine whether the formation of the granules requires microtubules, we examined the effect of vincristine, a microtubule inhibitor, on the cellular distribution of MB. To ensure that the effect of vincristine is not due to general inhibition of cell division, we injected vincristine in one of the cells at the 16-cell stage after the embryo had been injected with MB at the 1-cell stage and monitored the cellular distribution of MB in the

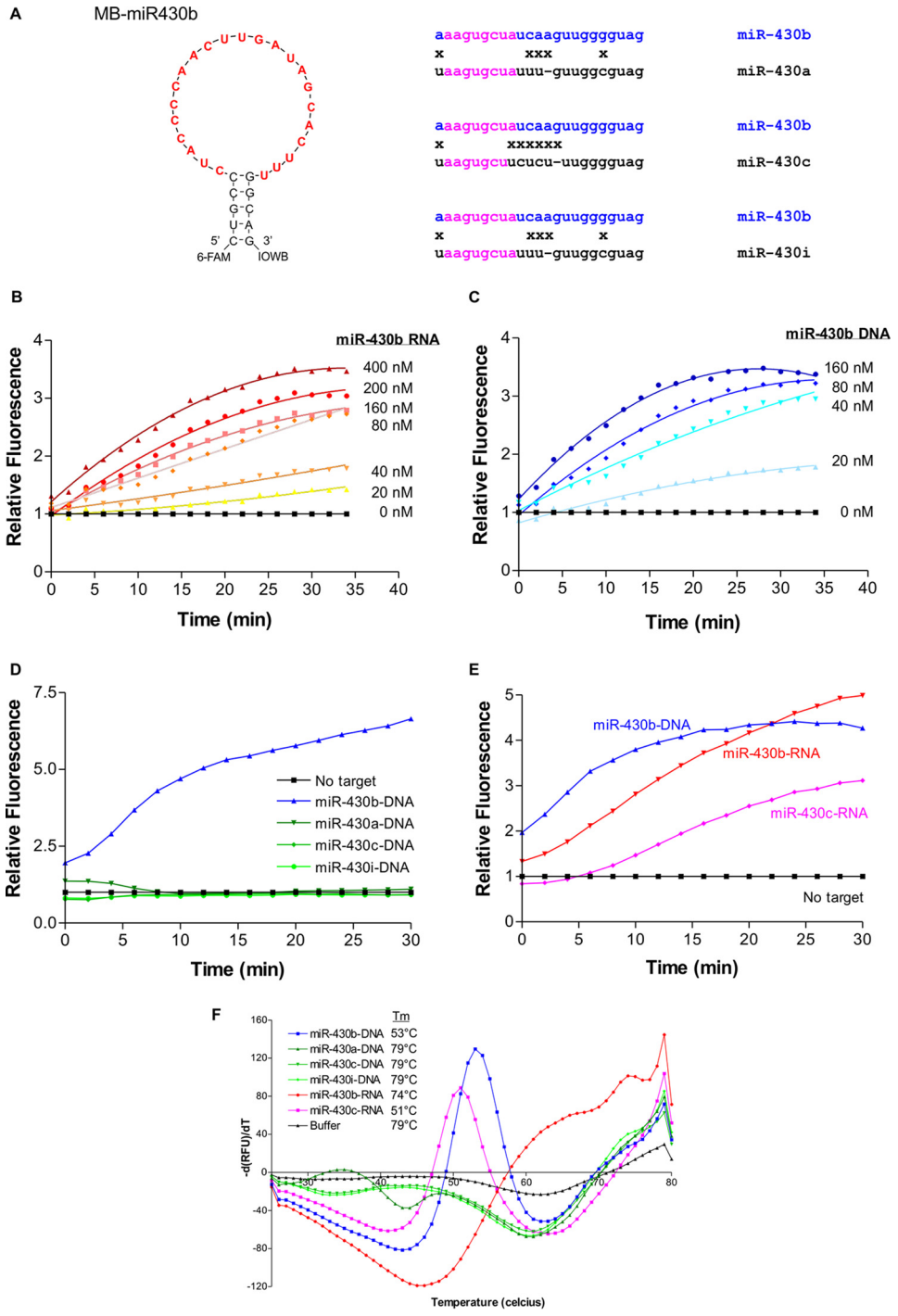

FIGURE 1. **Molecular beacon exhibits specificity toward miR-430b.** *A*, secondary structure of MB-miR430b with nucleotides shown in *red* indicating the region complementary to dre-miR-430b. Other members of the miR-430 family in zebrafish (*D. rerio*) are aligned with miR-430b for comparison. The seed sequence of each miRNA is shown in *pink*, whereas a mismatch is indicated by *x*. *B* and *C*, hybridization of MB to its RNA (*B*) or DNA (*C*) target is both concentration- and time-dependent. *D*, binding of MB toward its target made with DNA is highly sequence specific because none of miR-430a-DNA, miR-430c, or miR-430i (320 nM) exhibited any binding. *E*, however, MB can still bind to miR-430c-RNA (320 nM), although at a slower rate when compared with miR-430b-RNA. *F*, the binding of MB to its various target molecules was also analyzed by generating the melting curve with each target molecule.

embryo. As shown in Fig. 2*J*, granules were clearly visible in actively dividing cells (*arrowheads*). However, the formation of granules was completely abolished in cells which have completely stopped dividing (*red region*) as well as in cells that have not completely stopped dividing (*blue region*). These results suggest that granule formation is indeed sensitive to microtubule inhibition.

The important role of miR-430 in the degradation of maternal mRNAs during MZT has been shown previously (18). To investigate whether miR-430 is associated with the RNA degradation machinery, we carried out immunohistochemistry as well as *in situ* hybridization using whole embryos that had been previously injected with MB at the 1-cell stage and then fixed at 5 hpf. As shown in Fig. 2 (*L–N*), nuclear MB co-localized with

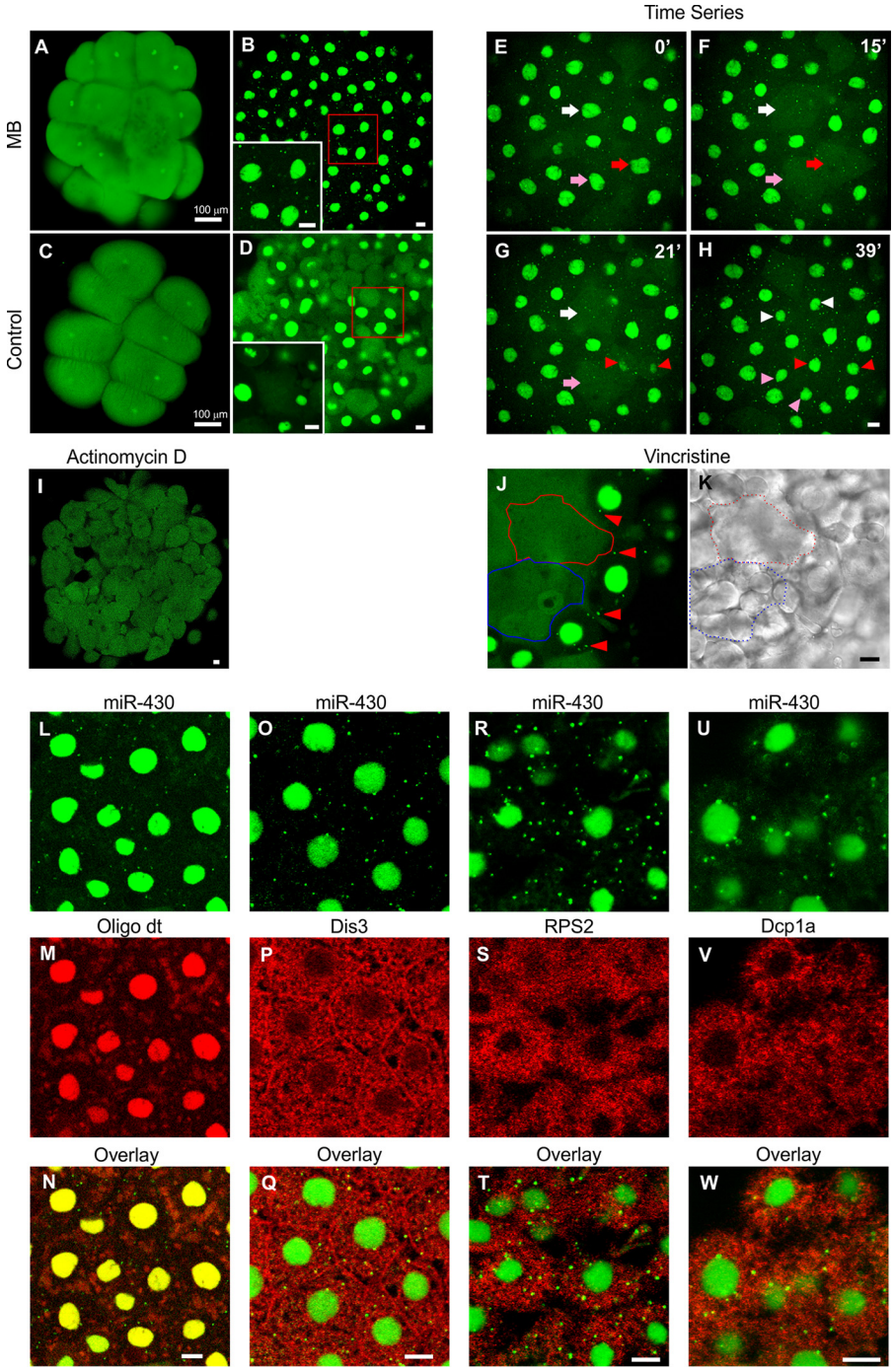

FIGURE 2. **Localization of MB in the developing zebrafish embryo.** *A–D*, MB and a control beacon were injected at the 1-cell stage and monitored from the 8-cell stage to 4 hpf to determine their cellular localization. Early in development, both beacons showed nuclear and cytoplasmic localization (*A* and *C*). *B* and *D*, at 4 hpf, MB was found to localize to both the nucleus and granules within the cytoplasm (*B*), whereas the control beacon remained predominantly in the nucleus (*D*). *E–H*, time lapse experiment was performed using spinning disk microscopy to further monitor the localization of MB throughout the cell division cycle after a zebrafish embryo was injected with MB at the 1-cell stage (0.03 ρmol). MB localization in the nucleus disappeared before nuclear division (*white*, *pink*, and *red arrows* in *E* and *F*) and reappeared in the newly formed nuclei of daughter cells (*red arrowheads* in *G* and *H* and *white* and *pink arrowheads* in *H*). *I*, to determine whether the nuclear signal was due to MB binding to DNA or miR-430 precursors, actinomycin D (3.2 ρmol) was co-injected with MB (0.05 ρmol) at the 1-cell stage to stop transcription. *J* and *K*, to determine whether the formation of the cytoplasmic granules were dependent on microtubules, a vincristine experiment was performed. Zebrafish embryo was first injected with MB at the 1-cell stage (0.02 ρmol) and subsequently injected with vincristine (0.025 ρmol) into one of the cells at the 16-cell stage to examine the localized effect of vincristine on MB localization. Some of the cells within the same embryo stopped dividing as a result of localized injection of vincristine (*red* and *blue regions*). Both nuclear and granular localization of MB was abolished in the same region (*J*), whereas cytoplasmic granules are clearly visible in neighboring cells that were still actively dividing (*J*, *arrowheads*). To determine whether MB is co-localized with any of the RNA degradation machinery, MB-injected embryos were fixed at 5 hpf and then probed with oligo(dT) (*L–N*) or immunostained for Dis3 (*O–Q*), RPS2 (*R–T*), or Dcp1a (*U–W*). *Scale bars*, 10 μm except for *A* and *C*.

oligo(dT), which hybridizes to the poly(A) tails of mRNAs. However, MB cytoplasmic granules were not associated with poly(A)-containing mRNAs in the cytoplasm. Dis3, an exosomal protein that exhibits both endoribonuclease and exoribonuclease activity, plays an important role in degrading RNA within the cell (25, 26). We found that MB localization was not associated with Dis3, which is known to be mainly distributed in the cytoplasm (Fig. 2, *O–Q*). Our results also showed that miR-430 did not co-localize with Dcp1a (Fig. 2, *U–W*), a decapping enzyme present in P-bodies, which are also known sites of mRNA turnover (27). Because miR-430 is known to stop translation before causing mRNA turnover (28), it may be possible that miR-430 is associated with ribosomes. We used RPS2 as a ribosomal marker and tested whether MB is co-localized with RPS2. As shown in Fig. 2 (*R–T*), RPS2 was distributed in the cytoplasm but not together with MB granules. In an attempt to further characterize the cytoplasmic localization of MB, we designed another molecular beacon to detect *Mknk2b* mRNA, which is a known target of miR-430. As shown in Fig. 3*B*, *Mknk2b* mRNA also formed cytoplasmic granules in addition to being in the nucleus. However, the formation of these granules did not completely match with that of miR-430, either temporally or spatially. The formation of miR-430 granules appeared ~1 h before that of *Mknk2b* mRNA (data not shown). In addition, not all of the miR-430 granules co-localized with *Mknk2b* mRNA granules (Fig. 3*A*) and vice versa (Fig. 3*B*). It is also interesting to note that some of these granules appeared to be in the process of merging together (Fig. 3*D*, *panels 1*, *2*, *4*, *9*, and *13*). As a negative control, we included another MB, which targets *Tnfaip1* mRNA, a known non-target of miR-430 (18). Unlike *Mknk2b* mRNA, which is a target of miR-430, *Tnfaip1* mRNA was not found in cytoplasmic granules (Fig. 3, *F* and *G*). Immunostaining of Dicer in MB-injected embryos showed that some of the miR-430 granules were also occupied by Dicer (Fig. 3, *H–K*), indicating that some of these granules co-localize with the miRNA biogenesis machinery. In summary, using a specific MB targeted to miR-430, we found that cytoplasmic miR-430 is localized in distinct granules that are shared by its target mRNA.

Developmental Defects Induced by MB—Based on the above findings that both molecular beacons (MB-miR430b and molecular beacon for piR-dre-210905) were localized to the nucleus, we were interested in using them for tracking cells in the developing embryo. With the use of lightsheet microscopy, we followed the development of embryos injected with either MB-miR430b (experimental) or piR-dre-210905 (control) at the beginning of the bud stage. Supplemental Movies S1 and S2 show the entire time lapse experiment, and stacked images from selected time points are shown in Fig. 4 (*A* and *B*). Convergent extension was clearly seen in both experimental and control embryos as cells migrated toward the dorsal midline. The formation of neural folds began at ~240 min for both experimental and control embryos (Fig. 4, *A* and *B*). However, MB-injected embryo failed to complete neural fold formation, which was evident at later time points (Fig. 4, *A*, *640′–820′*, and *D*), whereas control-injected embryo clearly developed neural folds at the end of the time lapse experiment (Fig. 4, *B*, *880′*, and *F*, *red arrows*). A 2D image of the MB-injected embryo at 24 hpf indicated the absence of a cavity in the brain, whereas the control embryo clearly developed a brain cavity at the same time period (Fig. 4, *C* and *E*). To further investigate brain ventricle formation, control and MB-injected embryos were fixed at 24 hpf, and the heads of the embryos were imaged using confocal microscopy. As shown in Fig. 4 (*G* and *I*), the control-injected embryo had developed a forebrain, midbrain, and hindbrain with distinct hollow cavities that were not present in the MB-injected embryo. At 48 hpf, MB-injected embryos clearly showed defects in development that were not restricted to the head area (Fig. 4, *H* and *J*).

The predominant role of miR-430 in brain development had been shown by a previous study using the MZ*dicer* mutants, which are defective in processing precursor miRNAs to mature miRNAs (23). Our results that MB injection can lead to brain development defects suggest that MB can inhibit the function of miR-430. To further investigate the developmental defects caused by MB, we conducted experiments using localized injection of MB. Thus, we injected MB randomly into one of the blastomeres at the 16-cell stage. Because the cell fate of the embryo is unknown at this development stage, we imaged the embryos at the shield stage, using spinning disk microscopy, to determine the location of the injected MB (Fig. 5*B*, *panels ii* and *iv*) relative to the embryonic shield (Fig. 5*B*, *panels i* and *iii*). Areas of precursor cells at the shield stage responsible for brain/notochord, circulation/blood, heart, and kidney development is illustrated in Fig. 5*A* according to Kimmel *et al.* (29) and Woo *et al.* (30). Injected embryos with MB localized in any of these four different areas at the shield stage were monitored for up to 7 days for defects observed under a light microscope. Examples of developmental defects in the brain (absence of hollow cavities), notochord (deformed tube structure), heart (continuous tube rather than formation of a distinct atrium and ventricle), and kidney (overall edema) are shown in Fig. 5*C*. Defects in circulation/blood development were scored by the complete absence of blood or blood movement in the embryo as observed under a light microscope. Table 1 summarizes the percentages of embryos having various developmental defects after localized injection of MB. In general, the type of developmental defects is highly correlated (70–95%) with MB accumulation in the specification region of the embryo.

MB Labeling Inhibits the Function of miR-430—The observed developmental defects suggested that the binding of MB to its target miRNA causes inhibition of the miRNA function. Because miR-430 plays an essential role in the clearance of maternal mRNAs during early embryonic development, we hypothesize that MB can increase the level of the target mRNAs of miR-430. To test this hypothesis, we extracted total RNA from untreated and MB-injected embryos at 48 hpf and measured the level of several mRNAs that have been shown to be targets of miR-430 (18). The level of *Mknk2b*, *Got2a*, and *CTZS* mRNA, as quantified by qPCR, was clearly elevated in embryos treated with MB, with *Mknk2b* mRNA having the highest effect. Derepression of these mRNAs confirms that MB, designed for use as a probe to detect miR-430, can also act as a strong inhibitor of this miRNA.

To determine the effectiveness of MB as a miR-430 inhibitor, we compared it with the standard anti-miR using morpholino

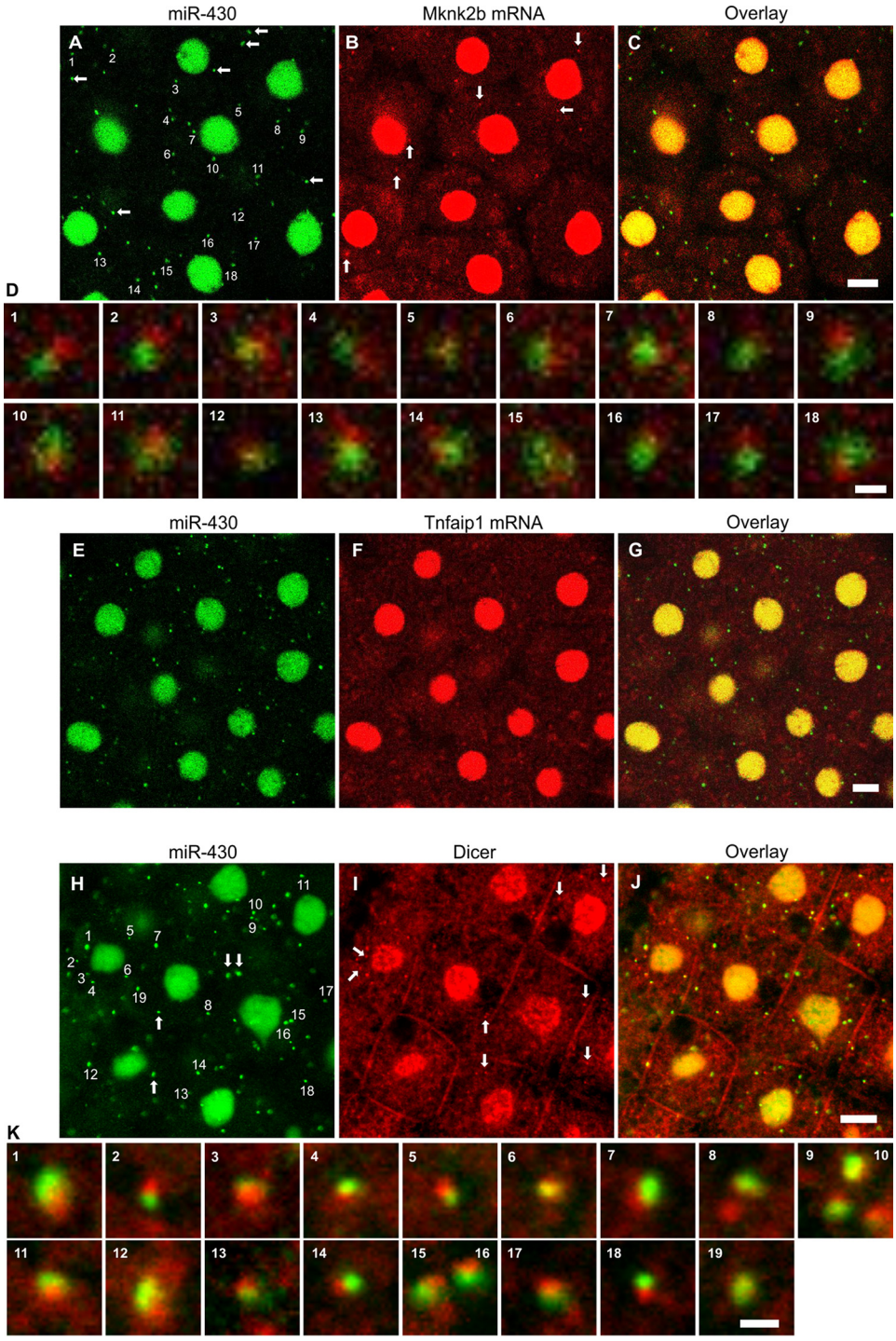

FIGURE 3. **Co-localization of miR-430 with its target mRNA and Dicer.** Molecular beacons targeted to *Mknk2b* or *Tnfaip1* mRNA were co-injected with MB-430b at the 1-cell stage, and the embryos were imaged between 5 and 6 hpf to study the cellular distribution of miR-430 (*A* and *E*), *Mknk2b* mRNA (*B*), or *Tnfaip1* mRNA (*F*). miR-430 clearly co-localized with *Mknk2b* mRNA both in the nucleus (*C*) and in some cytoplasmic granules, which are also shown in enlarged images in *D*. *Tnfaip1* mRNA, which is a non-target mRNA of miR-430, was found in the nucleus but not in cytoplasmic granules (*F* and *G*). MB-injected embryos were also fixed at 5 hpf and then immunostained for Dicer (*I*). Cytoplasmic granules stained positive for Dicer and MB are also shown in enlarged images in *K*. Not all miR-430 cytoplasmic granules co-localized with *Mknk2b* mRNA or Dicer (*arrows* in *A* and *H*) and vice versa (*arrows* in *B* and *I*). *Scale bars*, 10 μm in *C*, *G*, and *J* and 1 μm in *D* and *K*.

oligonucleotide with the same complementary region to miR-430 (MO). Using brain defects as an indicator of miR-430 inhibition (as shown in Figs. 5*C* and 6*B*), the dose response of both MB and MO were determined. As shown in Fig. 6*A*, 0.01 ρmol of MB could achieve 100% brain defects, whereas 2 ρmol of MO was needed to achieve the same effect, nearly 200-fold difference. Only when a high dose of MO was co-injected with MB into the embryos, localization of MB to cytoplasmic granules was inhibited, as a result of competition (Fig. 6*C*). This result further suggests that the cytoplasmic granules are occupied by mature miR-430. It is interesting to note that injection of MO could not compete with MB for binding to its targets in

the nucleus. This result suggests that the nuclear targets of MB are likely to be miR-430 precursors but not mature miR-430.

Discussion

In this study, we designed a molecular beacon to detect miR-430, a miRNA family that is highly expressed during early development in the zebrafish. Based on findings from previous work that molecular beacons with an RNA backbone have higher affinity than DNA or LNA backbone toward miRNA (16), we chose to use 2′-*O*-methyl RNA backbone for designing our MB-miR430b. Indeed, our *in vitro* results show that MB forms a more stable complex with its target having an RNA backbone than DNA backbone. In terms of sequence specificity,

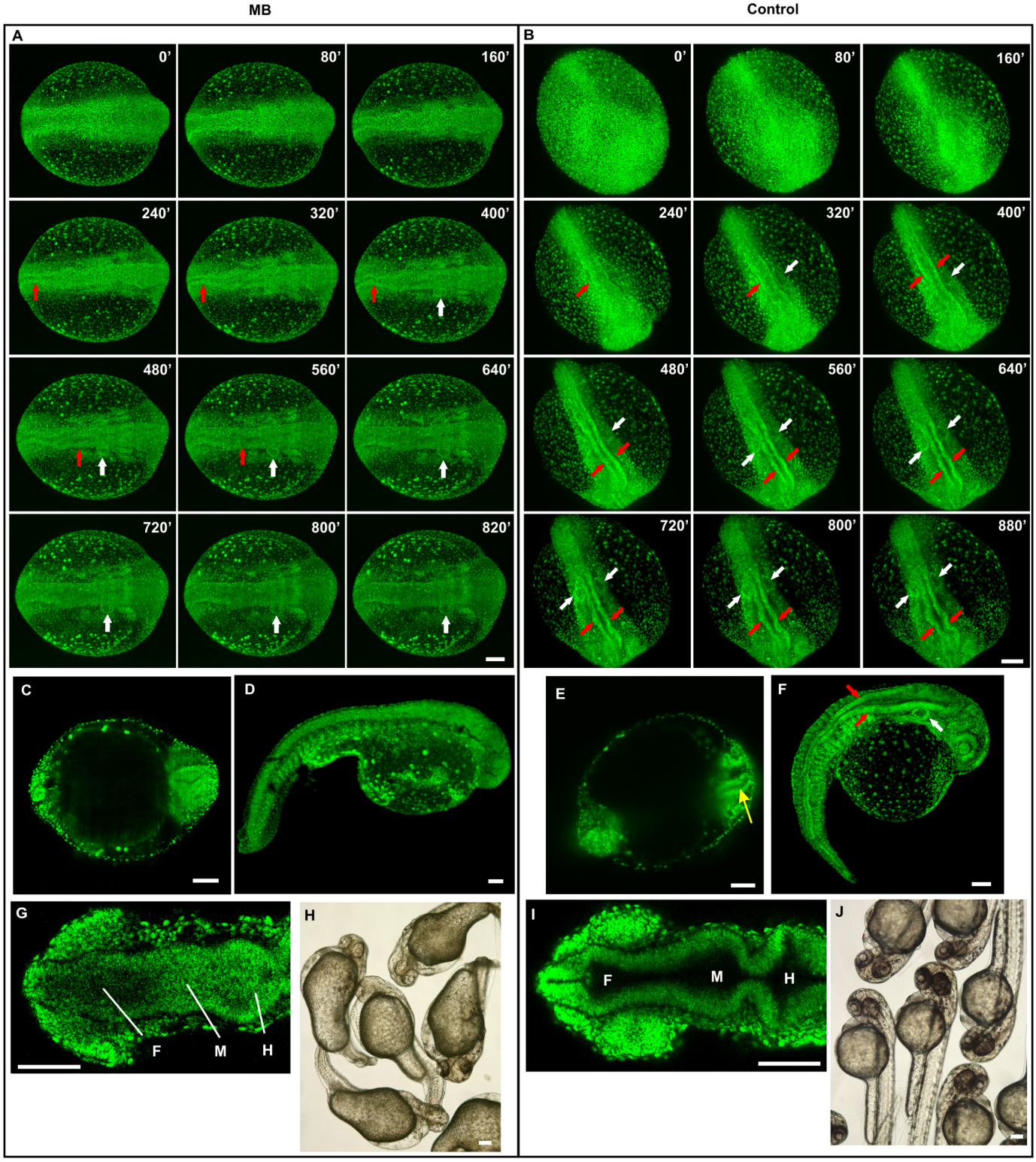

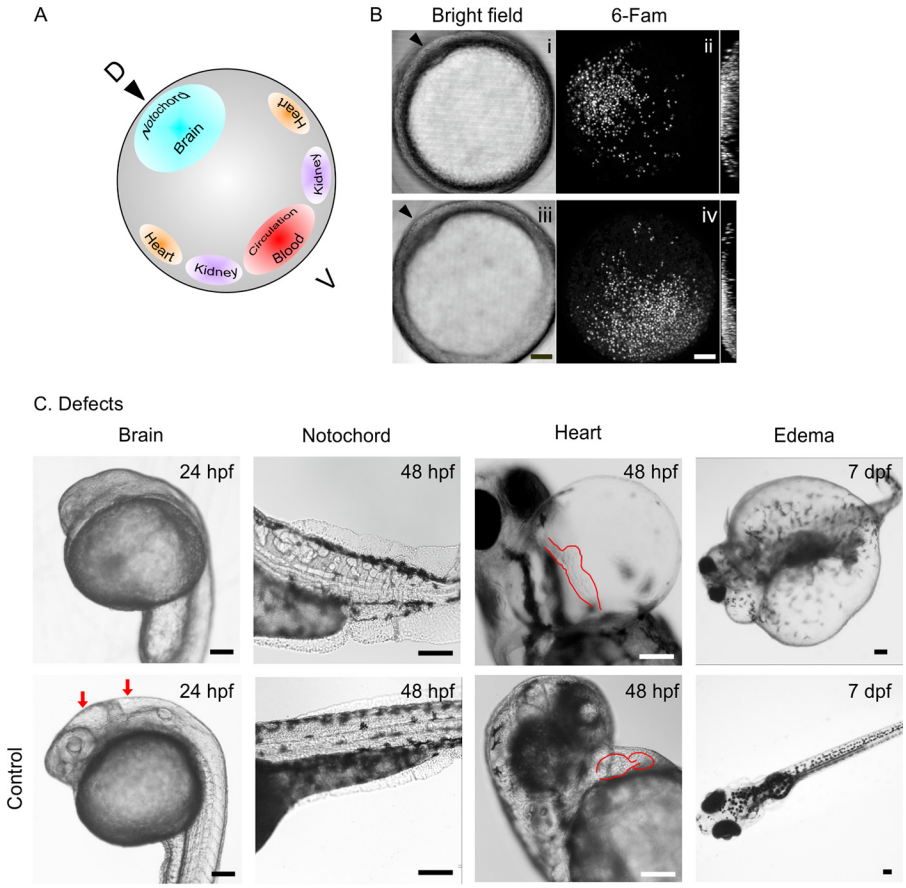

FIGURE 5. **Localized injection of MB caused various developmental defects.** Zebrafish embryos were injected with MB (0.01–0.02 ρmol) in one of the blastomeres at the 16-cell stage. The embryos were imaged using spinning disk microscopy at the shield stage to determine the localization of the injected MB. The areas of precursor cells in a shield stage embryo responsible for the future development of the brain, notochord, heart, kidney, blood, and circulation are shown in *A* based on Kimmel *et al.* (29). *D* denotes dorsal, and *V* denotes ventral. Examples of embryos with MB localized to the brain and notochord region (*top panels*), and in the heart, kidney, and blood/circulation region (*bottom panels*) are shown in *B*. The position of the embryonic shield (*black arrowheads*) is shown in the bright field images in *panels i* and *iii*. Stacked images showing MB localization of the same embryo as in *panels i* and *iii* are shown in *panels ii* and *iv*, respectively. The embryos were monitored for developmental defects from 1 to 7 dpf. Representative image of developmental defects in the brain, notochord, heart, and kidney are shown in *C*. *Red arrows* indicate brain ventricle, and the *red lines* are delineation of the heart. *Scale bars*, 100 μm.

TABLE 1

Localized injection of MB caused various developmental defects

	Developmental defects[a]			
	Brain/notochord	Heart	Kidney[b]	Blood/circulation[c]
True positive[d]	7/10 (70%)	17/18 (95%)	13/16 (81%)	10/12 (83%)
False positive[e]	0/13 (0%)	2/5 (40%)	4/7 (57%)	1/11 (9%)

[a] Zebrafish embryos were injected with MB locally and monitored for developmental defects from 1 to 7 dpf as described in Fig. 5.
[b] Defect in kidney function was scored by total body edema as shown in Fig. 5*C*.
[c] Defect in blood/circulation was scored by the complete absence of blood and movement in the circulation system when viewed under light microscope.
[d] True positive means embryos scored with developmental defects matched with the accumulation of MB in the specification region.
[e] False positive means embryos scored with developmental defects not matched with the accumulation of MB in the specification region.

FIGURE 4. **Brain developmental defects induced by MB.** A zebrafish embryo was injected with 0.01 ρmol of MB (*A*) or 0.1 ρmol of control beacon (*B*) and then imaged using a Carl Zeiss Lightsheet Z.1 microscope every 20 min from 10.5 hpf (late bud stage) to 24.5 hpf (*A*) or from 10 hpf (early bud stage) to 30 hpf (*B*). Stacked images from selected time points are shown. Neural folds (indicated by *red arrows*) can be clearly seen in the embryo injected with control beacon in the later part of the experiment, whereas it is absent in the embryo injected with MB. A 2D image of the same MB-injected embryo showed the absence of a lumen in the brain at 24 hpf (*C*), whereas the same control embryo clearly showed a lumen in the brain (*yellow arrow*) in the same time period (*E*). During the time lapse experiment, the embryo was immobilized in 1% low melting agarose and thus remained in a spherical shape. After imaging with the Lightsheet microscope, the embryo was alive, and when released from the agarose, it was allowed to return to its normal shape with its newly developed tail as imaged using a Zeiss LSM 710 confocal microscope (*D* and *F*). At 24 hpf, embryos were fixed (*G*), and 2D images (*I*) were obtained using confocal microscopy. The embryos injected with MB showed clear defects in brain ventricle development at 24 hpf (*G*), whereas control embryo developed brain morphology indicative of a forebrain, midbrain, and hindbrain (*I*). Bright field images of embryos injected with MB and control beacon at 48 hpf are shown in *H* and *J*, respectively. All images, except *G* and *I*, are images of live embryos. *Scale bars*, 100 μm. Otic vesicles are indicated by *white arrows* (in all panels). *F*, forebrain; *M*, midbrain; *H*, hindbrain.

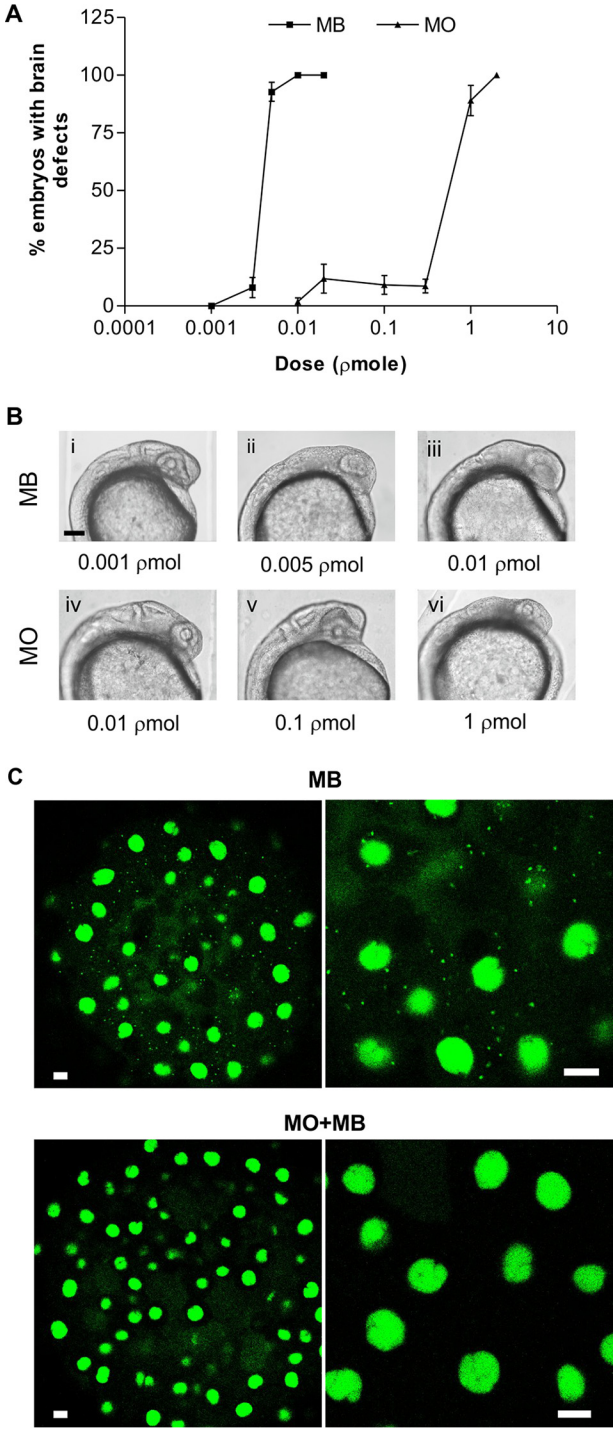

FIGURE 6. **MB is superior to MO in inhibiting miR-430.** Groups of 3–9 zebrafish embryos were injected with each of the indicated dose of MB or MO at the 1-cell stage and then monitored for brain defects at 24 hpf. *A*, dose response of MB and MO averaged from 4–7 replicate experiments ± S.D. *B*, representative embryos injected with the indicated dose of MB or MO showing hollow brain cavities (*panels i*, *iv*, and *v*) was scored as normal, whereas embryos with the absence of lumen in the brain area were scored as brain defects (*panels ii*, *iii*, and *vi*). *C*, co-injection of MO and MB. Injection of MO (3 ρmol) completely abolished MB localization in cytoplasmic granules. *Scale bars*, 100 μm in *B* and 10 μm in *C*.

MB-miR430b has the highest affinity toward targets that are fully complementary (miR-430b-RNA) but can still bind to other miR-430 members such as miR-430c-RNA with a much lower affinity. This finding suggests that MB can probably detect other members of miR-430 family when injected into zebrafish embryos.

Upon microinjection into the zebrafish embryo at the 1-cell stage, MB was found to distribute to two different intracellular compartments. Even as early as the 16-cell stage, MB was found to localize to the nucleus. When transcription was inhibited, this nuclear signal was completely abolished, suggesting that MB was not binding to the miR-430 genes. Starting at 4 hpf, around the time of MZT, punctate structures were observed throughout the cytoplasm. Competition experiments using miR-430 morpholino could only prevent MB localization to cytoplasmic granules but not to the nucleus. We propose that nuclear localization of MB is likely due to MB binding to the miR-430 precursors. The morpholino, which is made of DNA, is not likely to be as effective as MB in binding to miR-430 precursors. Although several mature miRNAs, including miR-29b, have been shown to localize to the nucleus (31–36), we think it is not the case for miR-430 because the hexanucleotide element that was found to direct miR-29b to the nucleus (31) is not present in miR-430. Cytoplasmic granules are presumably the turnover sites of the target mRNAs of miR-430. Because miR-430 is known to cause massive turnover of maternal mRNAs (18), co-localization of miR-430 with poly(A) mRNA was highly expected. However, our *in situ* hybridization experiments showed insignificant co-localization in the cytoplasm. Rather, our results clearly showed co-localization of miR-430 and *Mknk2b* mRNA in cytoplasmic granules. Our results also suggest that miR-430-directed turnover of mRNAs may employ a novel mechanism because none of the previously known RNA degradation machineries such as the exosome and P-bodies were found to co-localize with miR-430. Conversely, immunostaining experiments showed that some of these cytoplasmic granules were occupied with Dicer, an endoribonuclease involved in the maturation of microRNAs. In summary, our results indicate that at least some of the cytoplasmic granules are involved in the biogenesis of miR-430, and some granules are the functional site of miR-430 with its target mRNA.

Another novel finding from this study is the ability of specific molecular beacons to inhibit the function of the targeted miRNA based on the developmental defects observed. When MB was injected into the embryo at the 1-cell stage in an attempt to deliver the beacon to all of the cells, the most obvious phenotypic change observed was defects in brain ventricle development. This finding agrees with a previous report on the morphological function of miR-430 in brain development (23). When MB was administered into a more localized cell population, we observed morphological defects that are more related to the future fate of the cell population. In general, we grouped the defects into four different categories, including brain/notochord, heart, kidney, and blood/circulation. Accumulation of MB in cells at the dorsal region of the embryo mainly resulted in brain or notochord developmental defects, whereas accumulation of MB at the ventral midline resulted in blood/circulation defects. MB accumulation in cells located off the midline of the embryo resulted in defects indicative of heart and kidney development. We also performed rescue experiments by injecting MB premixed with miR-430b, but severe defects that are not restricted to the brain, heart, and blood/circulation develop-

TABLE 2
Effect of MB injection on the expression of genes regulated by miR-430b

Genes	ΔC_T[a,b]		$\Delta\Delta C_T$	Relative quantity (compared with control)[c]
	MB	Control		
Mknk2b	1.38 ± 1.6	3.89 ± 0.16	−2.52 ± 1.58	5.74 (1.90–17.1)
Got2a	6.38 ± 0.48	7.69 ± 0.34	−1.31 ± 0.48	2.48 (1.77–3.46)
CTZS	5.86 ± 0.69	7.25 ± 0.07	−1.40 ± 0.69	2.63 (1.63–4.24)

[a] Embryos were either left untreated (control) or injected with MB (0.02 pmol) at the 1-cell stage. At 48 hpf, embryos were collected in RNAlater for subsequent RNA extraction and quantification of gene expression by qPCR.
[b] Three to four biological replicates, with 25–30 embryos/replicate, were used to determine averaged ΔC_T ± S.D. using actin as the reference gene.
[c] Fold change in gene expression relative to control was determined by $2^{-\Delta\Delta CT}$ with the range indicated in parethenses.

ment were observed (data not shown). These results suggested nonspecific defects caused by the toxicity of dsRNA as demonstrated previously (37). Thus, rescue experiments were not a feasible option to confirm the inhibitory effects of MB on miR-430. As an alternative, we measured the levels of mRNAs that are known targets of miR-430, and indeed they were up-regulated in embryos injected with MB (Table 2). To our knowledge, this is the first study to demonstrate that miR-430 plays a diverse role in morphogenesis and is required in different progenitor populations to control gene expression in a spatial and temporal manner. Previous work using the MZ*dicer* mutants demonstrated that injection of miR-430 could only rescue the brain defects but not defects in heart, circulation, and ear development (23). We reason that the required amount of miR-430 in different progenitor cells is probably variable at different developmental stages, and a single injection of miR-430 at the 1-cell stage may not be sufficient to deliver the right amount of miR-430 to all different progenitor cells. Indeed, miR-430 was also shown to control germ cell migration at a later stage (38), further supporting a diverse role of miR-430 in embryonic development.

Currently, there are several strategies to study the loss of function of miRNAs, including genetic knock-out, miRNA sponges, anti-miR oligonucleotides, and target protectors (39). The latter two are more widely used in zebrafish and are made with morpholino oligonucleotides, which are resistant to nuclease and are target-specific. Anti-miR oligonucleotides are antisense to the mature miRNA of interest, whereas target protectors are oligonucleotides that are antisense to a specific target mRNA of the miRNA of interest (20, 38, 40–44). Hence, anti-miR oligonucleotides inhibit all the downstream function of the miRNA by inhibiting its interaction with the entire miRNA seed family of mRNAs, whereas target protectors are only inhibiting the specific interaction of a particular miRNA with one of its many target mRNAs. Because molecular beacons also contain a sequence that is antisense to its target miRNA, it is not surprising that it also has an inhibitory function. However, it is interesting to note that MB was a very potent miR-430 inhibitor. In this study, MB was found to be 2 orders of magnitude more potent than MO. The higher efficacy of molecular beacon as a miRNA inhibitor may be due to its secondary structure, which exposes the complementary sequence in a single-stranded loop. Inhibition of miRNAs inside the cell is probably more complicated than was envisioned. In the cytoplasm, mature miRNAs are found associated with cellular components for RNA silencing and degradation such as the P bodies and GW bodies (45). In these structures, miRNAs may already have bound mRNAs and are not very accessible for anti-miR binding. Having the complementary sequence in a single-stranded loop may increase the probability of the miRNA inhibitor to encounter with the target miRNA under *in vivo* conditions. Other anti-miR oligonucleotides and target protectors are not necessarily in a linear conformation and may form secondary structures that mask the complementary sequence. Another possible explanation for the higher efficacy of MB as a miRNA inhibitor is the RNA backbone instead of DNA backbone. As demonstrated in this study, RNA-RNA hybrid is more stable than DNA-RNA hybrid. Thus, this may explain why MB is able to bind better to miR-430 precursors than MO. As a result, MB may be a stronger miRNA inhibitor because of its ability to interfere with miR-430 biogenesis.

The use of molecular beacon as a miRNA sensor has been attempted in many studies using cell lines. However, it is difficult to determine whether the results obtained truly represent the localization of the miRNAs because of the method used for the intracellular delivery of these molecular beacons. Lipid-based delivery methods are notorious for delivery to the endocytic pathway and thus would bias the localization results. In fact, none of these studies reported any inhibitory effect of the molecular beacon on the miRNA. Perhaps, this is an indication that none of these studies were successful in using molecular beacon as a specific sensor in these systems. Our study showed for the first time, using zebrafish embryos and microinjection to bypass the obstacles in delivery, the success and usefulness of molecular beacon as a miRNA sensor. Our results clearly showed that, at least in the zebrafish model, molecular beacons can be employed to perform dual functions to detect a specific miRNA and as an miRNA inhibitor. Microinjection of molecular beacons into actively dividing cells has the advantage of delivering the oligonucleotide directly to both the cytoplasm and the nucleus because the nuclear envelop disassembles and reassembles with each short cell cycle during development. From the perspective of developing molecular beacon as a miRNA inhibitor, we propose that it is advantageous to have an inhibitor that acts earlier in the miRNA biogenesis pathway in addition to being a stronger decoy. From the perspective of using molecular beacon as a detector, the developmental defects induced can be used as confirmation of the sensor targeting the right miRNA.

Experimental Procedures

Materials—All molecular beacons, MB-miR430b, which is here referred to as MB (5′-6-FAM-CUGCCCUACCCCAACUUGAUAGCACUUUGGCAG-Iowa Black-3′), the control beacon for detecting piR-dre-210905 (5′-6-FAM-CUGCCAAAGCCAGCCAACUGCGUACGGCAG-Iowa Black-3′),

MB-c-Myc (5′-Cy3-CUGCCGGGGGCCUUUUCAUUG-UUUUCCCGGCAG-Black Hole Quencher-3′), MB-Mknk2b (5′-Cy3-CUGCCUUGAUAAAAGUGCUGCUGGCAG-Iowa Black-3′), and MB-Tnfaip1 (5′-Cy3-CUGCCAAAAAUGAG-GUAAAUAGGCAG-Iowa Black-3′) contain 2′*O*-methyl RNA bases and were purchased from IDT (Coralville, Iowa). DNA oligonucleotides corresponding to the sequences of miR-430a (5′-TAAGTGCTATTTGTTGGCGTAG-3′), miR-430b (5′-AAAGTGCTATCAAGTTGGGGTAG-3′), miR-430c (5′-TAAGTGCTTCTCTTTGGGGTAG-3′), and miR-430i (5′-TAAGTGCTATTTGTTGGCGTAG-3′) were purchased from IDT. 5′-Labeled Cy3-oligo(dT) (30-mer) and RNA oligonucleotides corresponding to miR-430b (5′-AAAGUGCUAU-CAAGUUGGGGUAG-3′) and miR-430c (5′-UAAGUGCUU-CUCUUUGGGGUAG-3′) were also purchased from IDT. Morpholino targeted to miR-430 (5′-CTACCCCAACTT-GATAGCACTTT-3′) was purchased from Gene Tools (Philomath, OR). Anti-Dis3 antibody (LS-C187155) was purchased from LifeSpan BioSciences, Inc. (Seattle, WA). Anti-RPS2 (N2C3) was obtained from Genetex (Irvine, CA). Anti-Dcp1a (AB2) was purchased from Sigma. Anti-Dicer (R13D6) was obtained from Clonegene.

Design of Molecular Beacons—The molecular beacons used in this study (MB, MB-c-Myc, MB-Mknk2b, and the control beacon for detecting piR-dre-210905) were designed as according to the published procedure of Bratu *et al.* (46) using 2′-*O*-methyl RNA bases. These small hairpins have a single-stranded loop region ranging from 17 to 23 nucleotides long and a double-stranded stem, which is 5 nucleotides long. A fluorophore and quencher is attached to the 5′ and 3′ end of the hairpins as illustrated in Fig. 1*A*.

Microinjection and Fixation of Embryos—Zebrafish embryos were microinjected at the 1-cell stage with MB (0.02–0.24 *ρ*mol) or the control beacon (0.002–0.3 *ρ*mol) to study miR-430 intracellular localization. A lower dose of MB (0.005–0.02 *ρ*mol) was injected either at the 1-cell stage or 16-cell stage to study developmental defects. No developmental defects were observed with control beacon injected as high as 0.3 *ρ*mol. Following injection, the embryos were incubated in 30% Danieau's solution at 28 °C to allow for development until microscopy or fixation. For fixation, embryos were manually dechorionated and then fixed in 4% paraformaldehyde at 4 °C overnight. After washing with PBS three times, the embryos were progressively dehydrated in methanol to reach 100% methanol in the final step, before long term storage (up to 1 year) at −80 °C until immunohistochemistry. For *in situ* hybridization, embryos were stored at −20 °C in 100% methanol for 1 h before rehydration progressively in PBS/methanol solutions to reach 100% PBS. After three washes in 2× SSC, the embryos were prehybridized at 37 °C for 1 h in 2× SSC with 50% formamide, 1% BSA, and tRNA (10 mg/ml). The embryos were then hybridized with Cy3-oligo(dT) (60 nM) in the same prehybridization solution at 37 °C for 16 h. After three washes with 2× SSC at 37 °C (5 min each), the embryos were imaged using confocal microscopy. For immunohistochemistry, the embryos were blocked overnight at 4 °C with 1% BSA in PBS containing 1% DMSO and then immunostained with either anti-Dis3 antibody (1:100), anti-RPS2 (1:200), or anti-Dcp1a (1:50) diluted in block buffer. Anti-rabbit Alexa Fluor 594 (diluted 1:200) was used as secondary antibody. After each immunostaining step with antibody, the embryos were washed three times in PBS containing 1% DMSO.

Hybridization Assay and Melt Curve—The binding of MB to various tested target molecules was carried out in a 384-well plate in 50 μl of buffer containing 10 mM Tris-Cl (pH 7.4), 50 mM NaCl, and 10 nM MB. Real time fluorescence signal was monitored using a Synergy™ 2 multidetection microplate reader (BioTek Instruments) immediately after the addition of the tested target molecules at concentrations indicated for each experiment. The binding of MB was also assessed by determining the melting temperature of MB with each of the target molecules using IQ™5 multicolor real time PCR detection system (Bio-Rad). In the experiment, 200 nM of MB and 1.6 μM of each target molecule were used in 25 μl of the binding assay buffer described above. After an initial denaturation step of 95 °C for 1 min, the temperature was lowered from 80 to 25 °C at a rate of 1 °C/min. The change in fluorescence signal, expressed as −d(RFU)/dT, was monitored as a function of temperature, and the melting temperature of the each hybrid was determined at the peak of −d(RFU)/dT. Representative results from three experiments are shown.

Microscopy—Bright field images in Figs. 4, 5*C*, and 6*B* were captured using a Nikon AZ100 Multizoom microscope. For Lightsheet microscopy, live embryos were immobilized in 1% low melting agarose prepared in Daneau's solution and maintained at 28 °C. The embryos were imaged using a Zeiss Lightsheet Z.1 microscope every 20 min with a total of 70 stacks captured at each time point (Fig. 4, *A–C* and *E*). Live imaging (Figs. 2, *E–H*, and 5*B*) was also performed using the spinning disk microscope (Carl Zeiss AxioObserver Z1 inverted microscope with a Yokogawa CSU-X1 spinning disk unit and an Andor iXon897BV EMCCD camera). The embryos were maintained at 28 °C on a heating stage, whereas images were captured using a 20× (Plan-Apochromat, 0.8 NA) objective lens and with iQ operation software (Andor Technology). All other 2D confocal images were obtained using either a LSM710 (Figs. 2*C* and 4, *D* and *F*), LSM780 (Fig. 2*A*), Leica SP5 (Figs. 2, *B*, *D*, and I–N, and 4, *G* and *I*), Olympus Fluoview FV1000 (Figs. 2, *O–W*, and 3, *H–K*), or Nikon C1 (Figs. 3, *A–G*, and 6*C* and supplemental Fig. S1) confocal laser scanning microscope.

Quantitative Real Time PCR—Embryos were injected with MB (0.02pmol) at the 1-cell stage. At 2 days postfertilization (dpf), between 20 and 40 embryos were collected into RNAlater solution (Ambion) and stored at −80 °C until total RNA extraction. RNA extraction was performed using the mirVana kit (Ambion). Prior to cDNA synthesis using the iScript kit (Bio-RAD), 500 ng of total RNA was subjected to DNA removal using the DNA-free™ kit (Ambion). qRT-PCR was performed to measure *Mknk2b*, *Got2a*, and *CTZS* mRNA levels using the following primers (5′ to 3′): Mknk2b: forward, ACACATT-TAGCCCCTACCGC, and reverse, GCAACAACGGTG-GTCTTAGC; Got2a: forward, GTCTTACAGCTCCG-GGCAAG, and reverse, ACACTGCTGAGGACGAATGG; and CTZS: forward, CACTAGTGCATTAGCAGATCG-TATCA, and reverse, CAATCACGTTCTGGACAGAGAGA. The thermal cycling protocol was according to previously

established procedures with an annealing temperature of 60 °C (47, 48).

Author Contributions—W. M. L. designed and conducted all of the experiments, analyzed the results, and wrote most of the paper. C.-M. C. conducted some of the experiments. A. L. M. and C. H. L. wrote the paper with W. M. L.

Acknowledgment—We thank Carl Zeiss Inc. for the use of the light-sheet microscope at Marine Biological Laboratory (Woods Hole, MA).

References

1. Pauli, A., Rinn, J. L., and Schier, A. F. (2011) Non-coding RNAs as regulators of embryogenesis. *Nat. Rev. Genet.* **12,** 136–149
2. Urbanek, M. O., Nawrocka, A. U., and Krzyzosiak, W. J. (2015) Small RNA detection by *in situ* hybridization methods. *Int. J. Mol. Sci.* **16,** 13259–13286
3. Politz, J. C., Zhang, F., and Pederson, T. (2006) MicroRNA-206 colocalizes with ribosome-rich regions in both the nucleolus and cytoplasm of rat myogenic cells. *Proc. Natl. Acad. Sci. U.S.A.* **103,** 18957–18962
4. Politz, J. C., Hogan, E. M., and Pederson, T. (2009) MicroRNAs with a nucleoar location. *RNA* **15,** 1705–1715
5. Kang, W. J., Cho, Y. L., Chae, J. R., Lee, J. D., Choi, K. J., and Kim, S. (2011) Molecular beacon-based bioimaging of multiple microRNAs during myogenesis. *Biomaterials* **32,** 1915–1922
6. Jo, M. H., Ali, B. A., Al-Khedhairy, A. A., Lee, C. H., Kim, B., Haam, S., Huh, Y. M., Ko, H. Y., and Kim, S. (2012) A reverse complementary multimodal imaging system to visualize microRNA9-involved neurogenesis using peptide targeting transferrin receptor-conjugated magnetic fluorescence nanoparticles. *Biomaterials* **33,** 6456–6467
7. Kang, W. J., Cho, Y. L., Chae, J. R., Lee, J. D., Ali, B. A., Al-Khedhairy, A. A., Lee, C. H., and Kim, S. (2012) dual optical biosensors for imaging microRNA-1 during myogenesis. *Biomaterials* **33,** 6430–6437
8. Lee, C. H., Chae, J., Ko, H. Y., and Kim, S. (2013) Molecular beacon-based microRNA biosensor for imaging EPC-treated cellular therapy of ischemia. *J. Mol. Imaging Dynam.* **2,** 113–123
9. Choi, Y. S., Kim, H. S., Woo, J., Hwang, E. H., Cho, K., Kim, S., and Moon, W. K. (2014) Real-time imaging of the epithelial-mesenchymal transition using microRNA-200a sequence-based molecular beacon-conjugated magnetic nanoparticles. *PLoS One* **9,** 1–10
10. Ko, H. Y., Lee, J., Lee, Y. S., Gu, H. N., Ali, B. A., Al-Khedhairy, A. A., Heo, H., Cho, S., and Kim, S. (2015) Bioimaging of the microRNA-294 expression dependent color change in cells by a dual fluorophore-based molecular beacon. *Chem. Comm.* **51,** 2159–2161
11. Tyagi, S., and Kramer, F. R. (1996) Molecular beacons: probes that fluoresce upon hybridization. *Nat. Biotechnol.* **14,** 303–308
12. Hernandez, R., Orbay, H., and Cai, W. (2013) Molecular imaging strategies for *in vivo* tracking of microRNAs: a comprehensive review. *Curr. Med. Chem.* **20,** 3594–3603
13. Ko, H. Y., Hwang, D. W., Lee, D. S., and Kim, S. (2009) A reporter gene imaging system for monitoring microRNA biogenesis. *Nat. Protoc.* **4,** 1663–1669
14. Kato, Y., Miyaki, S., Yokoyama, S., Omori, S., Inoue, A., Horiuchi, M., and Asahara, H. (2009) Real-time functional imaging for monitoring miR-133 during myogenic differentiation. *Int. J. Biochem. Cell Biol.* **41,** 2225–2231
15. Kato, Y., Sawata, S. Y., and Inoue, A. (2010) A lentiviral vector encoding two fluorescent proteins enables imaging of adenoviral infection via adenovirus-encoded miRNAs in single living cells. *J. Biochem.* **147,** 63–71
16. Baker, M. B., Bao, G., and Searles, C. D. (2012) *In vitro* quantification of specific microRNA using molecular beacons. *Nucleic Acids Res.* **40,** e13
17. Wei, C., Salichos, L., Wittgrove, C. M., Rokas, A., and Patton, J. G. (2012) Transcriptome-wide analysis of small RNA expression in early zebrafish development. *RNA* **18,** 915–929
18. Giraldez, A. J., Mishima, Y., Rihel, J., Grocock, R. J., Van Dongen, S., Inoue, K., Enright, A. J., and Schier, A. F. (2006) Zebrafish miR-430 promotes deadenylation and clearance of maternal mRNAs. *Science* **312,** 75–79
19. Lund, E., Liu, M., Hartley, R. S., Sheets, M. D., and Dahlberg, J. E. (2009) Dedadenylation of maternal mRNAs mediated by miR-427 in *Xenopus laevis* embryos. *RNA* **15,** 2351–2363
20. Choi, W. Y., Giraldez, A. J., and Schier, A. F. (2007) Target protectors reveal dampening and balancing of nodal agonist and antagonist by miR-430. *Science* **318,** 271–274
21. Rosa, A., Spagnoli, F. M., and Brivanlou, A. H. (2009) The miR-430/427/302 family controls mesendodermal fate specification via species-specific target selection. *Dev. Cell* **16,** 517–527
22. Wienholds, E., Kloosterman, W. P., Miska, E., Alvarez-Saavedra, E., Berezikov, E., de Bruijn, E., Horvitz, H. R., Kauppinen, S., and Plasterk, R. H. (2005) MicroRNA expression in zebrafish embryonic development. *Science* **309,** 310–311
23. Giraldez, A. J., Cinalli, R. M., Glasner, M. E., Enright, A. J., Thomson, J. M., Baskerville, S., Hammond, S. M., Bartel, D. P., and Schier, A. F. (2005) MicroRNAs regulate brain morphogenesis in zebrafish. *Science* **308,** 833–838
24. Thatcher, E. J., Bond, J., Paydar, I., and Patton, J. G. (2008) Genomic organization of zebrafish microRNAs. *BMC Genomics* **9,** 253–261
25. Lebreton, A., Tomecki, R., Dziembowski, A., and Séraphin, B. (2008) Endonucleolytic RNA cleavage by a eukaryotic exosome. *Nature* **456,** 993–996
26. Chlebowski, A., Lubas, M., Jensen, T. H., and Dziembowski, A. (2013) RNA decay machines: the exosome. *Biochim. Biophys. Acta* **1829,** 552–560
27. Arribas-Layton, M., Wu, D., Lykke-Andersen, J., and Song, H. (2013) Structural and functional control of the eukaryotic mRNA decapping machinery. *Biochim. Biophys. Acta* **1829,** 580–589
28. Bazzini, A. A., Lee, M. T., and Giraldez, A. J. (2012) Ribosome profiling shows that miR-430 reduces translation before causing mRNA decay in zebrafish. *Science* **336,** 233–237
29. Kimmel, C. B., Warga, R. M., and Schilling, T. F. (1990) Origin and organization of the zebrafish fate map. *Development* **108,** 581–594
30. Woo, K., Shih, J., and Fraser, S. E. (1995) Fate maps of the zebrafish embryo. *Curr. Opin. Genet. Dev.* **5,** 439–443
31. Hwang, H. W., Wentzel, E. A., and Mendell, J. T. (2007) A hexanucleotide element directs microRNA nuclear import. *Science* **315,** 97–100
32. Place, R. F., Li, L. C., Pookot, D., Noonan, E. J., and Dahiya, R. (2008) MicroRNA-373 induces expression of genes with complementary promoter sequences. *Proc. Natl. Acad. Sci. U.S.A.* **105,** 1608–1613
33. Liao, J. Y., Ma, L. M., Guo, Y. H., Zhang, Y. C., Zhou, H., Shao, P., Chen, Y. Q., and Qu, L. H. (2010) Deep sequencing of human nuclear and cytoplasmic small RNAs revelas and unexpectedly complex subcellular distribution of miRNAs and tRNA 3′ trailers. *PLoS One* **5,** e10563
34. Jeffries, C. D., Fried, H. M., and Perkins, D. O. (2011) Nuclear and cytoplasmic localization of neural stem cell microRNAs. *RNA* **17,** 675–686
35. Khudayberdiev, S. A., Zampa, F., Rajman, M., and Schratt, G. (2013) A comprehensive characterization of the nuclear microRNA repertoire of post-mitotic neurons. *Front. Mol. Neurosci.* **6,** 43
36. Salmanidis, M., Pillman, K., Goodall, G., and Bracken, C. (2014) Direct transcriptional regulation by nuclear microRNAs. *Int. J. Biochem. Cell Biol.* **54,** 304–311
37. Zhao, Z., Cao, Y., Li, M., and Meng, A. (2001) Double-stranded RNA injection produces nonspecific defects in Zebrafish. *Dev. Biol.* **229,** 215–223
38. Staton, A. A., Knaut, H., and Giraldez, A. J. (2011) miRNA regulation of Sdf1 chemokine signaling provides genetic robustness to germ cell migration. *Nat. Genet.* **43,** 204–211
39. Stenvang, J., Petri, A., Lindow, M., Obad, S., and Kauppinen, S. (2012) Inhibition of microRNA function by antimiR oligonucleotides. *Silence* **3,** 1–17
40. Flynt, A. S., Li, N., Thatcher, E. J., Solnica-Krezel, L., and Patton, J. G. (2007) Zebrafish miR-214 modulates Hedgehog signaling to specify muscle cell fate. *Nat. Genet.* **39,** 259–263

41. Kloosterman, W. P., Lagendijk, A. K., Ketting, R. F., Moulton, J. D., and Plasterk, R. H. (2007) Targeted inhibition of miRNA maturation with morpholinos reveals a role for miR-375 in pancreatic islet development. *PLoS Biol.* **5,** e203
42. Martello, G., Zacchigna, L., Inui, M., Montagner, M., Adorno, M., Mamidi, A., Morsut, L., Soligo, S., Tran, U., Dupont, S., Cordenonsi, M., Wessely, O., and Piccolo, S. (2007) MicroRNA control of Nodal signaling. *Nature* **449,** 183–188
43. Leucht, C., Stigloher, C., Wizenmann, A., Klafke, R., Folchert, A., and Bally-Cuif, L. (2008) MicroRNA-9 directs late organizer activity of the midbrain-hindbrain boundary. *Nat. Neurosci* **11,** 641–648
44. Zeng, L., Carter, A. D., and Childs, S. J. (2009) miR-145 directs intestinal maturation in zebrafish. *Proc. Natl. Acad. Sci. U.S.A.* **106,** 17793–17798
45. Cheng, C. J., Saltzman, W. M., and Slack, F. J. (2013) Canonical and non-canonical barriers facing antimiR cancer therapeutics. *Curr. Med. Chem.* **20,** 3582–3593
46. Bratu, D. P., Catrina, I. E., and Marras, S. A. E. (2011) Tiny molecular beacons for in vivo mRNA detection. In *RNA Detection and Visualization: Methods and Protocols, Methods in Molecular Biology* (Gerst, J. E., ed) pp. 141–157, Humana Press, New York
47. Sleep, E., Boue, S., Jopling, C., Raya, M., Raya, A., and Izpisua Belmonte, J. C. (2010) Transcriptomics approach to investigate zebrafish heart regeneration. *J. Cardiovasc. Med.* (*Hagerstown*) **11,** 369–380
48. Dhanasiri, A. K., Fernandes, J. M., and Kiron, V. (2013) Liver transcriptome changes in zebrafish during acclimation to transport-associated stress. *PLoS One* **8,** e65028